Self-assembled insect muscle bioactuators with long term function under a range of environmental conditions

Article *in* RSC Advances · August 2014

DOI: 10.1039/C4RA08438A

CITATIONS
5

READS
27

5 authors, including:

Amanda Baryshyan
Conagen Inc.
5 PUBLICATIONS **60** CITATIONS
SEE PROFILE

Laura Domigan
Tufts University
12 PUBLICATIONS **101** CITATIONS
SEE PROFILE

Barry Andrew Trimmer
Tufts University
123 PUBLICATIONS **2,983** CITATIONS
SEE PROFILE

Published in final edited form as:
RSC Adv. 2014 January 1; 4(75): 39962–39968. doi:10.1039/C4RA08438A.

Self-assembled insect muscle bioactuators with long term function under a range of environmental conditions

A.L. Baryshyan[*,a], **L.J. Domigan**[*,a], **B. Hunt**[a], **B.A. Trimmer**[b], and **D. L. Kaplan**[a]

[a]Department of Biomedical Engineering, Tufts University. Medford, MA 02155, USA

[b]Department of Biology, Tufts University. Medford, MA 02155, USA

Abstract

The use of mammalian muscles as device actuators is severely limited by their sensitivity to environmental conditions and short lifetime. To overcome these limitations insect muscle stem cells were used to generate organized 3D muscle constructs with significant enhancements in environmental tolerance and long term function. These tissues self-assembled, self-repaired, survived for months in culture without media replenishment and produced stresses of up to 2 kPa, all under ambient conditions. The muscle tissues continued to function for days even under biologically extreme temperature and pH. Furthermore, the dimensions and geometry of these tissues can be easily scaled to MEMS or meso-scale devices. The versatility, environmental hardiness and long term function provide a new path forward for biological actuators for device needs.

Introduction

In recent years, muscle tissue engineering has been explored for applications beyond the field of regenerative medicine, including as biological motors or bioactuators [1], with applications in microelectromechanical systems (MEMS) and robotic devices [2, 3, 4]. Most tissue engineered bioactuators have used mammalian cardiac or skeletal muscle cells combined with specific growth substrates. For example, gel-mediated cell condensation around micropillars, microcontact printing of flexible membranes, and poly(N-isopropylacrylamide) (PIPAAm)-released cell sheets have generated structures that can perform deflection, curling or pumping actions, respectively [5, 6, 7]. Crawling- and swimming-type locomotion has also been demonstrated with free-standing devices [8, 9]. These strategies can provide a range of bio-mimetic motion and simplify the manufacture of micro-scale actuators by exploiting the ability of cells to self-assemble and to coordinate contraction and function. Furthermore, cell-based bioactuators may have utility over synthetic systems because of their potential for self-repair, tunable biodegradability, and use

[**]Please direct correspondence to david.kaplan@tufts.edu.
[*]The authors contributed equally to this work.

[c]Address here.

Electronic Supplementary Information (ESI) available: [details of any supplementary information available should be included here]. See DOI: 10.1039/b000000x/

of biocompatible fuel sources such as sugars and fats [1, 10]. However, a major limitation of systems comprised of mammalian cells is their need for stringent controls of temperature, pH, and oxygen for survival and function.

As an alternative, explanted insect tissues have been studied for their tolerance to ambient temperatures and a wide range of pH and oxygen conditions [4, 11]. However, these explants are restricted in size and it is difficult to reconfigure them for different applications. Furthermore, the use of excised tissues requires fine microdissection for each device, limiting scalability and leading to poor reproducibility.

In the present study, we used a bottom-up bioengineering approach to generate free-standing 3D muscle tissues via self-assembly from embryonic *Manduca sexta (M. sexta)* muscle stem cells (Fig. 1), based on methods previously established by our group [12]. The goal was to mimic the simple structure of insect muscle and retain desirable properties of the native tissues, along with resistance to environmental perturbations.

Experimental

Cell isolation and seeding

Egg harvesting, culture medium preparation, and cell isolations were performed as previously described [12]. All reagents were purchased from Invitrogen (Carlsbad, CA) or Sigma-Aldrich (St. Louis, MO), unless otherwise indicated. Briefly, eggs laid within a three hour period were collected from a *Manduca sexta* colony. The eggs were incubated for an additional 19 hours at 26°C. After 19 hours of incubation, embryos were counted, washed with dH_2O and sterilized in 25% bleach for 2 minutes. Embryos were then washed thoroughly with sterile water. Culture medium was prepared with 70% Leibovitz's L15 medium, 18% Grace's Insect Medium, 12% fetal bovine serum (FBS), 3.4 mg/mL yeast extract, 3.4 mg/mL lactalbumin hydrolysate (MP Biomedicals, Solon, OH), 0.37 mg/mL α-ketoglutaric acid, 1.21 mg/mL D (+)-glucose monohydrate, 0.67 mg/mL malic acid, 60 μg/mL succinic acid, 60 μg/mL imidazole, 1% Anti-Anti, 0.5% 1X RPMI 1640 vitamin mix, 0.5% 1X RPMI 1640 amino acid mix, and 20 ng/mL 20-hydroxyecdysone (20-HE). Medium was sterile filtered before use and the pH was adjusted to 6.5 with sterile 1M NaOH. The embryos were rinsed with media before transfer to a 7 mL Dounce homogenizer (Wheaton, Millville, NJ). Cells were released by lysing the embryos using plunger B. The homogenate was centrifuged twice, each for 5 minutes at 85 × g to remove excessive yolk material and pellet the cells. The pellet was then resuspended in medium and plated at a density of 27 615 cells/cm^2 into PDMS chambers.

Immunofluorescence staining and imaging

Immunostained samples were prepared as described previously [12]. Briefly, samples were fixed in 10% neutral buffered formalin (NBF), permeabilized in 1 wt% bovine albumin serum (BSA) and 0.05 wt% saponin, and blocked in 1 wt% BSA with 10% goat serum. Samples were then incubated overnight at 4°C in primary antibody (waterbug flight muscle myosin 1:4 in permealization buffer; Babraham Institute, Cambridge, UK). Samples were washed twice with PBS before incubation with AlexaFluor 555 F(ab')2 fragment of goat

anti-mouse IgG (1:200 dilution) and DAPI (1:1000 dilution). Samples were washed with PBS before visualizing using a Leica fluorescence microscope or confocal microscope.

Self-healing

Muscle tissues were generated as described above. After 14 days of culture, a 1-mm section of each experimental tissue was removed using a sterile blade and sterile microscissors. Images were collected before and after injuries were induced, and at regular intervals thereafter. Cell infiltration into the wound area was analyzed using ImageJ software.

Metabolic evaluation

Metabolic analyses were carried out on 30 day old constructs over a two week period. During the experimental period contraction was also monitored (see Contraction Evaluation) to ensure metabolic activity of actively contracting constructs was being captured. During the two week period media samples (60 μL from a total media volume of 2.5 mL) were taken at designated timepoints and glucose, protein, triglyceride and lactate concentrations assayed. Glucose assays were carried out using the Glucose (GO) Assay kit (Sigma). Protein assays were carried out using the BCA Protein Assay kit (Pierce). Triglyceride assays were carried out using the EnzyChrom Triglyceride Assay kit (BioAssay Systems, Hayward, CA). Extracellular lactate was evaluated using the EnxyChrom L-Lactate Assay kit (BioAssay Systems, Hayward, CA). All metabolic assays were carried out in 96-well plates using a plate reader (Molecular devices SpectraMax M2) according to the manufacturer's protocols.

LIVE/DEAD staining and imaging

Cultures were initiated using the methods described above. At designated timepoints, cultures were stained using a LIVE/DEAD kit, according to the manufacturer's instructions.

Environmental tolerance

After two weeks of culture at 26°C, videos were acquired for all experimental constructs to record spontaneous contractions. 3 videos were taken per construct at 10X magnification and 1280 × 960 pixel resolution. Video frames were captured at 600ms intervals, and 8 frames were acquired for each video. Samples were either replaced at 26°C, or switched to a humidified incubator at 37°C or 15°C. For samples where pH was being investigated, media was replaced with media that had been adjusted to the appropriate pH (5.5, 6.5, 7.5) and samples maintained at 26 °C. Negative controls were constructs fixed in 10% NBF for 45 minutes at room temperature. At each timepoint, videos were again acquired from each construct and used for index of movement (IOM) analysis. IOM analysis was performed as described previously using ImageJ [12]. To generate pseudocolored images, the first frame from each video was subtracted from the remaining seven to generate seven absolute value images. These were then added together to create a single differential image, which was then pseudocolored on a scale from 0 to 256. The areas of the pseudocolored images with the highest values correspond to the regions where the greatest change in pixel intensity, and therefore the most movement, occurred during the 4.8s video. For IOM quantification, average pixel intensity for each absolute value image was quantified and summated to

generate a single IOM value for that video. IOM values were averaged across 3 videos per construct, and the mean and standard deviation for each condition was calculated.

Chamber preparation

3D printed master molds for casting PDMS chambers were fabricated by designing molds using the CAD software Solidworks. The designs were printed using an Objet Connex500 3D printer with the Objet VeroClear™ material. The printed templates were thoroughly washed with water to remove the support material. The molds were dried and coated with Mann Ease Release 200 mold release spray. Sylgard 184 silicone elastomer (PDMS, Dow Corning, Midland, MI) was prepared according to the manufacturer's instructions. Approximately 1 g per mold of uncured silicone elastomer was added to each mold. The molds were degassed in a vacuum chamber prior curing at 60° C for 6 hours. The chambers were then removed and further modifications such as filters for further yolk removal or addition of silk sutures carried out where desired. For filter incorporation two holes are made at the ends of the channels using a size 3-biopsy punch. Nylon net filters with 10 um pores are cut to fit over the holes. The filters are fixed in place by DAP 100% Silicone Adhesive to create a watertight seal around the filter. Ethanol sterilized silk sutures are placed approximately 1 cm apart in culture dish. The PDMS chambers are placed over the sutures. The PDMS chambers are sterilized with 70% ethanol overnight and washed with sterile PBS for 48 hours. Remaining PBS is aspirated from and around the PDMS channels to secure the channels to the dish.

Spontaneous contractions tracked with time

Spontaneous contractile activity was tracked with time using IOM analysis. IOM was quantified as described for Environmental Tolerance above for at least 3 constructs per timepoint, using at least two videos per construct.

Contraction evaluation

Indirect tracking of spontaneous contractions were performed using IOM analysis, as described above. The spontaneous contraction force was measured using a silicon beam micro-force sensor with ion diffused resisters (AE801, SensorOne Technologies Corporation, Sausalito, CA). A small tungsten micro-hook was bonded to the surface of the silicon beam using cyanoacrylate adhesive and the sensor body was mounted on a micromanipulator so that the beam was vertical and perpendicular to the applied force. The paired sensor resisters were assembled into a half Wheatstone bridge configuration and the output signal recorded directly using a digital recording interface (PowerLab 26T, AdInstruments Inc, Colorado Springs, CO). The sensor was calibrated using known weights loaded in the same direction as the muscle contractions. The electrical response was linear over the sensitive range. The micro hook was gently lowered into one-end of the muscle construct loop and slowly moved to take up any slack. The reported stress is calculated from the force measured and the cross sectional area of the muscle construct.

Statistics

All assays were performed with a minimum sample size of n=3. Experimental groups were compared using a two-sided Student's t-test in Microsoft Excel. Statistically significant values are defined as indicated.

Results and Discussion

Muscle construct formation and characterization

Insect muscle tissues were generated using a simple molding technique whereby cells were seeded and confined within polydimethylsiloxane (PDMS) chambers, which were molded from 3D printed inverse chambers. Multiple geometries were fabricated, such as multifiber arrays with three contractile muscle fibers as one operable unit (Fig. 1A-B), designed to mimic the structure of *in vivo* larval muscle (Fig. 1Biii). Using this approach, contractile 3D muscle structures formed over several days within the chambers (Fig. 1Bi; S1). As shown in Fig, 1Bii, the PDMS chamber can easily be removed and organized engineered muscle fibers remain intact, attached to pins or sutures at the ends (Fig. 2B)). Our insect cell-based approach displayed several distinguishing characteristics not achievable with mammalian cell systems. For example, the muscle cells self-assembled into 3D structures without the need to be embedded in a hydrogel or other extracellular matrix (ECM) materials, which is often required for tissue condensation and integrity [13]. Using the insect hormone 20-hydroxyecdysone (20-HE) as a supplement in the growth media [14] promoted the growth of muscle cells as shown by positive myosin staining (Fig. 1C). Similar to mammalian muscle, mature insect muscle shows sarcomeric striations, as verified by our previously published full characterization of this cell system [12].However, other cell types contributed to the formation of organized tissues, for example, the secretion of native ECM by epithelial cells (Fig. S2), which in *M. sexta* generate matrix for muscle cell insertion in the underlying cuticle [15].

As the insect muscle tissues developed (Fig. 1D; videos available in Supplementary Materials), spontaneous contractile activity was observed. Initially, individual cells and groups of cells pulsed continuously (Fig 1D). This movement was monitored using video analysis to calculate overall Index of Movement (I.O.M.) reflecting changes in the duration and relative amplitude of the contractions. Activity slowed after two weeks, presumably due to cell fusion and muscle network formation (Fig. 1D).

Spontaneous contractile activity significantly increased from day 21 to day 30; with the entire tissue construct contracting in a coordinated fashion. (Fig. 1D) and by day 30, the muscle tissue had condensed and formed a functional bioactuator unit.

Muscle construct design and force production

Tissue size and geometry were controlled based on the shape and size of the PDMS chamber, such that I-bars, rings, and eyelets were generated (Fig. 2A), offering a range of actuator formats. In order to effectively guide muscle cell alignment, and thereby maximize coordination and force output, the width of the chamber channels was optimized to 500μm

to guide cellular alignment (Fig. S3). This corresponded to the dimensions of insect muscle fibers found *in vivo*, around 300μm in width (Fig. 1C).

Different biomaterials can be incorporated as end points or “artificial tendons”. These anchorage points allow for attachment of the muscles to substrates and devices, and enable transfer and handling of engineered tissues Silk sutures and stainless steel pins were used to this purpose (Fig. 2B). Materials were placed in the chambers prior to cell seeding. The cells grew around the structures and adhered tightly.

The force generation of our engineered tissues was measured both indirectly and directly, using I.O.M. analysis and a micro-force transducer, respectively. A representative trace from indirect measurements showed that contractions were typically 2 – 4 seconds in duration, and tended to display a double-peak (Fig. 2C). Force production of mature tissues (>d30) was assessed using a solid-state micro force transducer (Fig. 2D). The spontaneous movements frequently consisted of double-peak forces similar to those seen in the video analysis (Fig. 2E). The double-peak may be an indication of the presence of stretch-responsive fibers, or other physical or chemical connectivity within the network, such as muscle gap junctions or paracrine signaling [16]. The individual contractions produced stress in the range of 2 kPa (Fig. 2E), which translates to forces production on the same scale as has been observed for some mammalian bioactuators [2, 17].

Self-repair and long-term survival of insect muscle constructs

During insect myogenesis, developing muscle fibers reach out and are attracted to tendon-like cell precursors, which eventually anchor the muscle fibers to the larval body wall [18]. We wanted to see if a similar process was possible *in vitro*, as this could lead to self-healing capabilities in the constructs, as well as anchoring of bioactuators within devices. A 1-mm defect introduced into a preformed muscle partially repaired itself within one month, and contraction resumed in the repaired region (Fig. 3A). Muscle cells grew into the defect and migrated toward the opposite side of the resected region. Slow migration of a few cells was initially observed and after 30 days, cell elongation and further migration resulted in defect repair of approximately 40% (Fig. 3B). A restoral of full function upon complete defect repair is hypothesized although unknown at present. Although this process took several weeks to complete, it could potentially be accelerated by chemically attracting muscle stem cells or by increasing the cellular organization within the constructs.

M. sexta muscle cells cultivated *in vitro* survive for several months in the absence of medium replenishment [12]. Despite potential diffusion limitations in our 3D system, the *in vitro* cultured muscle tissues also thrived without changes in media over at least 90 days; with the majority of muscle cells were still viable by LIVE/DEAD staining (Fig. 3C). This result is in major contrast to mammalian cell systems, which require medium exchanges every 2 to 3 days to maintain viability [2, 3, 5, 6]. Three possible fuel sources, glucose, protein, and triglycerides, were assessed over a two-week period to elucidate the metabolic strategy used by these tissues to survive. The extracellular levels of these metabolites were not significantly depleted over this time period in mature (greater than 30 days old) contracting tissues (Fig. 3D, Fig. S4A). One possible explanation is *in vitro* production or mobilization of stored energy substrates by adipocyte or yolk cells present in the cultures,

which resulted in maintenance of fuel despite energy use and end-product production (Fig. S4). Yolk cells are maternally derived and are present from the initiation of the cultures, as previously shown [12]. Adipocytes differentiate after muscle in the *M. sexta* embryo, but may develop within the cultures [19].

Environmental tolerance of insect muscle constructs

In addition to long-term, maintenance-free viability, another desirable feature of bioactuators is pH and temperature tolerance and versatility. The spontaneous contractile activity of the muscle tissues at pH 5.5, 6.5 and 7.5 was assessed, along with a range of temperatures. Temperatures examined were 26°C, close to room temperature; human body temperature (37°C); and 15°C. The insect muscle tissues displayed sustained contractions at all three pH and temperatures values (Fig. 4). Therefore, unlike mammalian derived systems, *M. sexta* bioactuators are excellent candidates for applications at fluctuating ambient temperatures, and at human body temperature and pH.

Conclusions

Tissue engineered insect muscle bioactuators were generated using a simple method of cell guidance with PDMS templates. The use of embryonic cells without cell type separation allowed the developing tissues to self-assemble and function without additional intervention. In future work, methods may be developed to reduce the maturation time of the engineered muscle tissue to aid bioactuator production. Although force production could be enhanced with increased number of parallel fibers and electromechanical stimulation, a baseline level of stress production was observed in the absence of these refinements that is comparable to previously reported bioactuator output. In addition to having contractile function, these tissues were able to self-repair, survive for months without medium changes, and continue to survive and function under a wide range of temperature and pH conditions. As a result, insect bioactuators demonstrate potential to have utility in devices that require long-term function under varying environmental conditions.

Supplementary Material

Refer to Web version on PubMed Central for supplementary material.

Acknowledgments

We thank the NIH (P41 EB002520) (DLK), NSF (IOS-7045912) (BAT), and DARPA (BAA 10-65) (DK and BAT) for support of this work. The authors would also like to acknowledge Jelena Rnjak-Kovacina for input into method development and Rod Jose for graphical assistance.

References

1. Ricotti L, Menciassi A. Bio-hybrid muscle cell-based actuators. Biomed Microdevices. 2012; 14:987–998. [PubMed: 22960907]
2. Fujita H, Dau VT, Shimizu K, Hatsuda R, Sugiyama S, et al. Designing of a Si-MEMS device with an integrated skeletal muscle cell-based bio-actuator. Biomed Microdevices. 2011; 13:123–129. [PubMed: 20957437]

3. Choi E, Lee SQ, Kim TY, Chang H, Lee KJ, et al. MEMS-based power generation system using contractile force generated by self-organized cardiomyocytes. Sens Actuators, B. 2010; 151:291–296.
4. Akiyama Y, Sakuma T, Funakoshi K, Hoshino T, Iwabuchi K, et al. Atmospheric-operable bioactuator powered by insect muscle packaged with medium. Lab Chip. 2013; 13:4870–4880. [PubMed: 24185263]
5. Feinberg AW, Feigel A, Shevkoplyas SS, Sheehy S, Whitesides GM, et al. Muscular thin films for building actuators and powering devices. Science. 2007; 317:1366–1370. [PubMed: 17823347]
6. Hoshino T, Imagawa K, Akiyama Y, Morishima K. Cardiomyocyte-driven gel network for bio mechano-informatic wet robotics. Biomed Microdevices. 2012; 14:969–977. [PubMed: 23053450]
7. Tanaka Y, Soto K, Shimizu T, Yamato M, Okano T, et al. A micro-spherical heart pump powered by cultured cardiomyocytes. Lab Chip. 2007; 7:207–212. [PubMed: 17268623]
8. Chan V, Park K, Collens MB, Kong H, Saif TA, et al. Development of miniaturized walking biological machines. Sci Rep. 2012; 2:857–864. [PubMed: 23155480]
9. Nawroth JC, Lee H, Feinberg AW, Ripplinger CM, McCain ML, et al. A tissue-engineered jellyfish with biomimetic propulsion. Nat Biotech. 2012; 30:792–797.
10. Chan V, Asada HH, Bashir R. Utilization and control of bioactuators across multiple length scales. Lab Chip. 2014; 14:653–670. [PubMed: 24345906]
11. Akiyama Y, Iwabuchi K, Furukawa Y, Morishima K. Long-term and room temperature operable bioactuator powered by insect dorsal vessel tissue. Lab Chip. 2009; 9(1):140–144. [PubMed: 19209346]
12. Baryshyan AL, Woods W, Trimmer BA, Kaplan DL. Isolation and maintenance-free culture of contractile myotubes from *Manduca sexta* embryos. PLOS One. 2012; 7(2):e31598. [PubMed: 22355379]
13. Vandenburgh HH, Del Tatto M, Shansky J, LeMaire J, Chang A, et al. Tissue engineered skeletal muscle organoids for reversible gene therapy. Hum Gene Ther. 1996; 7:2195–2200. [PubMed: 8934233]
14. Luedeman R, Levine RB. Neurons and ecdysteroids promote the proliferation of myogenic cells cultured from the developing adult legs of *Manduca sexta*. Dev Biol. 1996; 173:51–68. [PubMed: 8575638]
15. Nardi JB. Embryonic origins of the two main classes of hemocytes – granular cells and plamatocytes – in *Manduca sexta*. Dev Genes Evo. 2004; 214(1):19–28.
16. Tamarkin DA, Levine RB. Synaptic interactions between a muscle-associated proprioceptor and body wall muscle motor neurons in larval and adult *Manduca sexta*. J Neurophys. 1996; 76(3): 1597–1610.
17. Horiguchi H, Imagawa K, Hoshino T, Akiyama Y, Morishima K. Fabrication and evaluation of reconstructed cardiac tissue and its application to bio-actuated microdevices. IEEE Trans Nanobiosci. 8:349–355.
18. Becker S, Pasca G, Strumpf D, Min L, Volk T. Reciprocal signaling between Drosophila epidermal muscle attachment cells and their corresponding muscles. Development. 124:2615–2622. [PubMed: 9217003]
19. Haunerland NH. Transport and utilization of lipids in insect flight muscles. Comp Biochem Physiol. 1997; 117B:475–482.

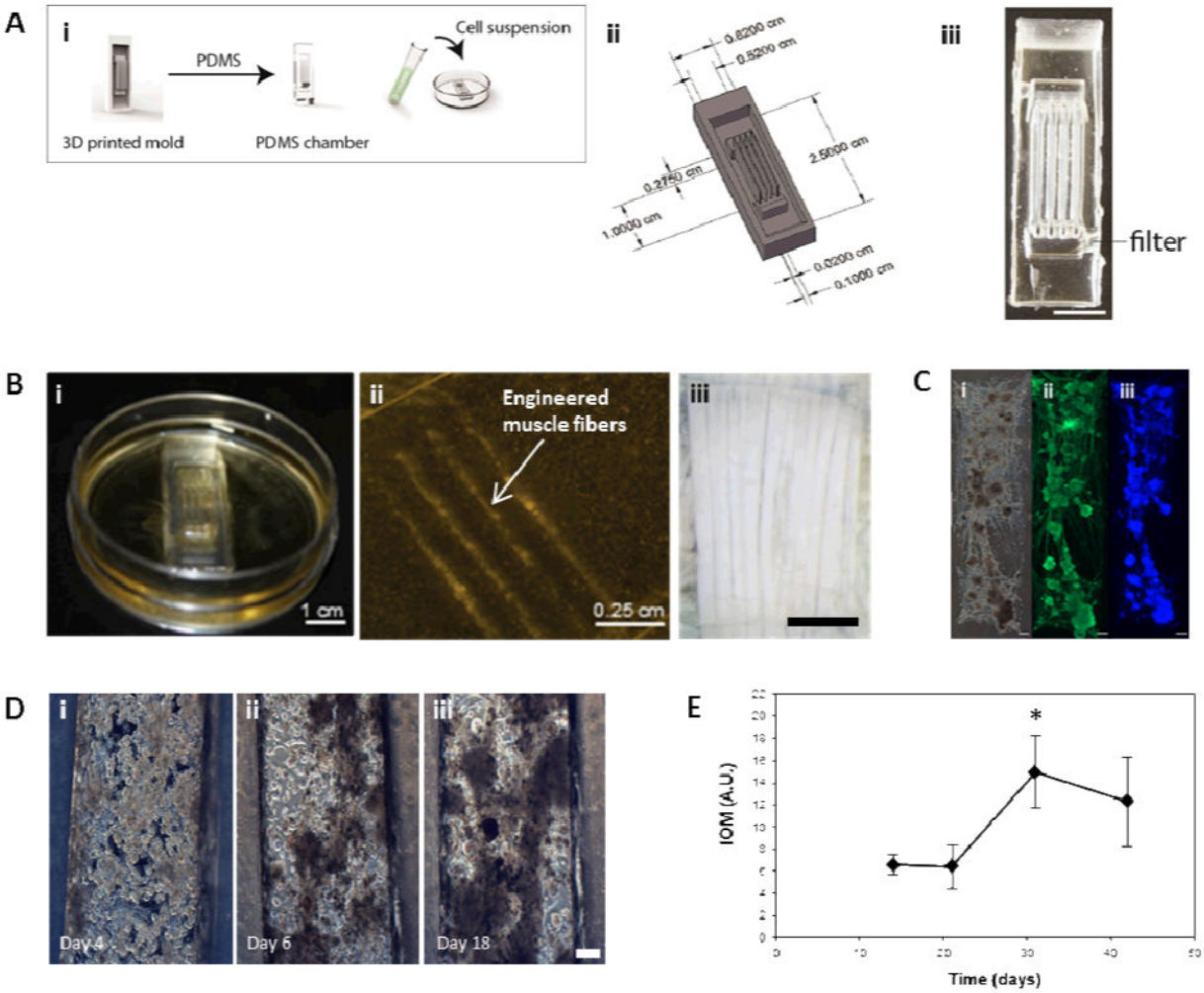

Figure 1. Muscle construct formation and characterization

(A) (i) Schematic showing the formation of scaffold free insect muscle tissues. Inverse seeding chamber molds were designed to the desired dimensions using SolidWorks, and arrays of these 3D printed. PDMS was cast into the mold arrays, producing a tissue chamber. A high density cell suspension was dropped on top of the chamber and contractile 3D constructs were then allowed to develop over time. (ii) Schematic and image (iii) of the multifiber seeding chambers used. Scale bar is 1 cm. (B) Macroscopic (i), and microscopic (ii) images of 3D muscle constructs, which aim to mimic the structure of native insect muscle, in this case larval *M. sexta* muscle fibers, an image of which is shown in (iii). Scale bars are 1 cm, 0.25 cm, and 1 mm, respectively. (C) Myosin staining confirming the presence of muscle fibers in the constructs. Shown are phase (i), and fluorescent images showing myosin (muscle, ii) and DAPI (nuclei, iii) staining. Scale bars are 200 μm. (D) Phase contrast microscopy images showing the formation of 3D muscle constructs via self-assembly from embryonic *M. sexta* muscle stem cells. Scale bar is 150 μm. (E) Index of movement (I.O.M.) analysis showing spontaneous contractile activity of developing cell constructs.

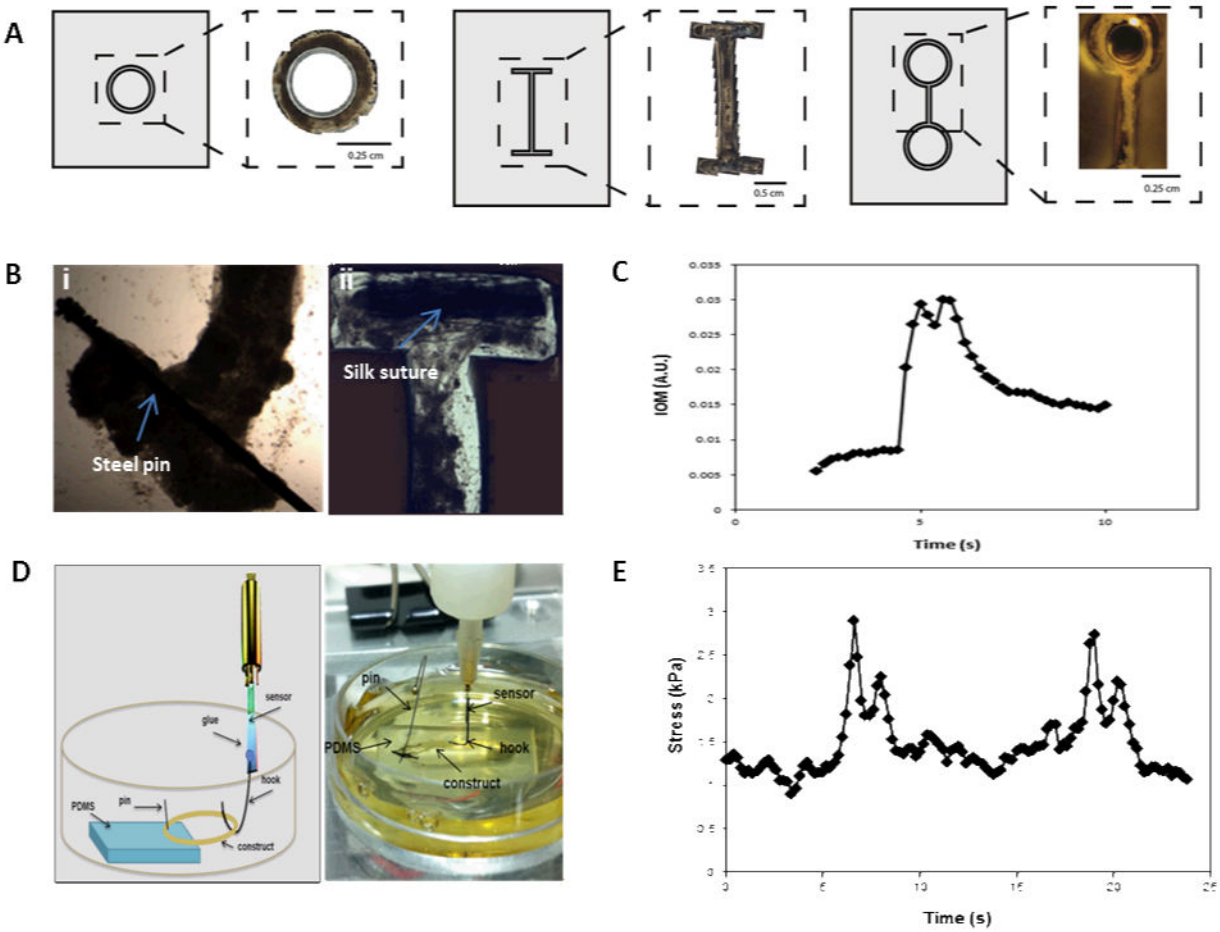

Figure 2. Muscle construct design and force production

(A) Tissue size and geometry were controlled by the shape of the seeding chamber such that a range of formats including rings (i), I-bars (ii), and eyelets (iii) were generated. (B) Biomaterials such as silk sutures (i) and stainless steel pins (ii) were also able to be incorporated. (C) Indirect measurement of force production via index of movement (I.O.M.) analysis showing a single contraction in real-time of a contractile tissue construct. (D) Schematic (left) and image (right) showing the set-up for direct force measurements using a customized solid-state force transducer. Briefly, a circular construct is attached at one end to a piece of PDMS with an insect pin and held taut via a hook attached to the force transducer. The construct is kept submerged in media throughout force recordings. (E) The contractile tissue network produces stress in the range of 2 kPa, as measured by a custom-built solid-state micro force transducer.

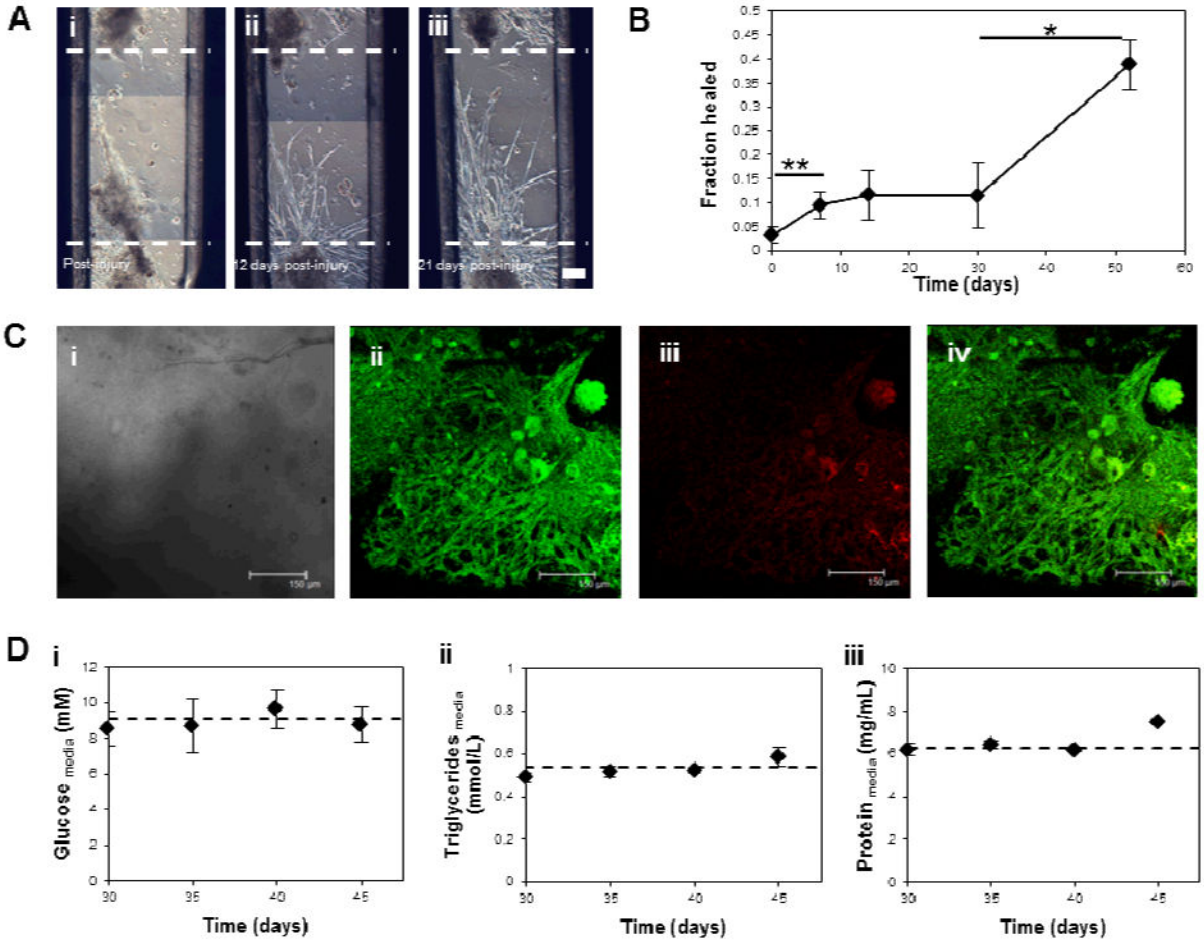

Figure 3. Self-repair and long-term survival of insect muscle constructs

(A) Phase construct images showing an "injured" muscle construct (i), and the migration of cells into the wounded area post-injury (ii, iii). Scale bar is 150 μm. (B) Quantification by image analysis of the self-repair capabilities of muscle constructs, shown as the fraction of the wounded area healed over time. (C) Confocal microscopy images showing survival of 90 day old tissue constructs via LIVE/DEAD staining. Images shown are (i) phase contrast, (ii) calcein AM fluorescence (live cells), (iii) ethidium homodimer-1 fluorescence (dead cells), and a merge (iv). Scale bars are 150 μm. (D) Extracellular levels of candidate fuel sources over a 20 day contractile period of 30 day old mature tissue constructs. Graphs show extracellular glucose (i), triglyceride (ii), and protein (iii) levels. The dotted line represents the level present in the media at day 1.

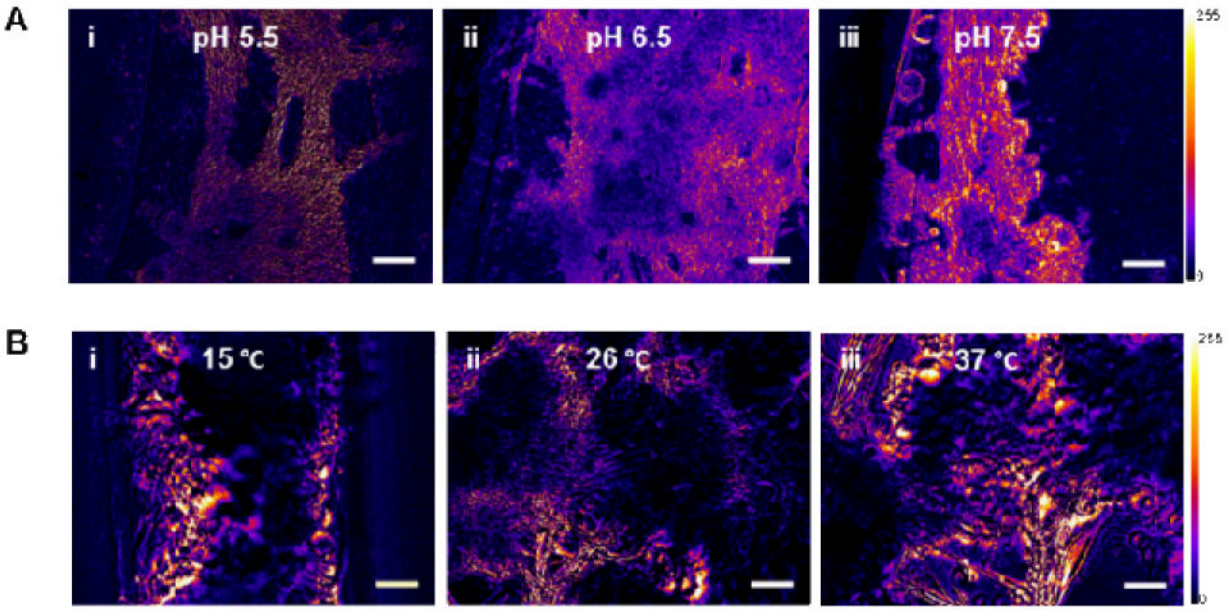

Figure 4. Environmental tolerance of insect muscle constructs

Pseudo-colored heat maps constructed using ImageJ analysis of videos of mature insect muscle constructs showing areas of contractile activity via change in pixel intensity (Scale shown). (A) Insect muscle construct contractile activity after 5 days at pH 5.5, 6.5, and 7.5. (B) Insect muscle construct contractile activity after 5 days at 15, 26, and 37 °C. Heat maps (i-iii), and phase constrast microscopy (iv-vi) images are shown. Scale bars are 100 μm.